Available online at www.sciencedirect.com

ScienceDirect

Solar Energy 131 (2016) 235–245

SOLAR ENERGY

www.elsevier.com/locate/solener

Theoretical investigation considering manufacturing errors of a high concentrating photovoltaic of cassegrain design and its experimental validation

Katie Shanks [a,*], Nabin Sarmah [b], Juan P. Ferrer-Rodriguez [c], S. Senthilarasu [a], K.S. Reddy [d], Eduardo F. Fernández [c], Tapas Mallick [a,*]

[a] Environmental and Sustainability Institute, University of Exeter Penryn Campus, Penryn TR10 9FE, UK
[b] Department of Energy, Tezpur University, Tezpur, Assam 784 028, India
[c] Centre for Advanced Studies in Energy and Environment, University of Jaen, Campus las Lagunillas, Jaen 23071, Spain
[d] Heat Transfer and Thermal Power Laboratory, Department of Mechanical Engineering, Indian Institute of Technology Madras, Chennai 600 036, India

Received 13 November 2015; received in revised form 4 February 2016; accepted 24 February 2016
Available online 9 March 2016

Communicated by: Associate Editor Igor Tyukhov

Abstract

A compact high concentrating photovoltaic module based on cassegrain optics is presented; consisting of a primary parabolic reflector, secondary inverse parabolic reflector and a third stage homogeniser. The effect of parabolic curvatures, reflector separation distance and the homogeniser's height and width on the acceptance angle has been investigated for optimisation. Simulated optical efficiencies of 84.82–81.89% over a range of ±1° tracking error and 55.49% at a tracking error of ±1.5° were obtained. The final singular module measures 169 mm in height and 230 mm in width (not including structural components such as cover glass). The primary reflector dish has a focal length of 200 mm and is a focal with the secondary inverse reflector which has a focal length of 70 mm. The transparent homogenising optic has a height of 70 mm, an entry aperture of 30 × 30 mm and an output aperture of 10 × 10 mm to match the solar cell. This study includes an analysis of the optical efficiency, acceptance angle, irradiance distribution and component errors for this type of concentrator. In particular material stability and the surface error of the homogeniser proved to be detrimental in theoretical and experimental testing – reducing the optical efficiency to ~40%. This study proves the importance of material choice and simulating optical surface quality, not simply assuming ideal conditions. In the experimental testing, the acceptance angle followed simulation results as did the optical efficiency of the primary and secondary reflectors. The optical efficiency of the system against increasing solar misalignment angles is given for the theoretical and experimental work carried out.
© 2016 The Authors. Published by Elsevier Ltd. This is an open access article under the CC BY license (http://creativecommons.org/licenses/by/4.0/).

Keywords: Concentrator photovoltaics; Optics; Ray trace simulation; Experimental testing

1. Introduction

Solar concentrator systems are an expanding research topic with various applications and benefits. Concentrator photovoltaic (CPV) designs have been pushing higher concentration ratios to achieve higher conversion efficiencies and cost effectiveness (Gordon et al., 2004; Languy and

* Corresponding authors.
E-mail addresses: Kmas201@exeter.ac.uk (K. Shanks), nabin@tezu.ernet.in (N. Sarmah), jferrer@ujaen.es (J.P. Ferrer-Rodriguez), S.Sundaram@exeter.ac.uk (S. Senthilarasu), KSReddy@iitm.ac.in (K.S. Reddy), fenandez@ujaen.es (E.F. Fernández), T.K.Mallick@exeter.ac.uk (T. Mallick).

http://dx.doi.org/10.1016/j.solener.2016.02.050
0038-092X/© 2016 The Authors. Published by Elsevier Ltd.
This is an open access article under the CC BY license (http://creativecommons.org/licenses/by/4.0/).

Habraken, 2013; Yavrian et al., 2013). However, the higher the concentration ratio of a solar concentrator system, the more dependent upon accuracy it becomes. This includes manufacturing accuracy and solar tracking accuracy. The relationship between concentration ratio and acceptance angle directly follows from etendue and is explained further by Gordon et al. (2008), Goldstein and Gordon (2011), Welford and Winston (1989). When comparing the types of solar concentrator photovoltaics, the Fresnel lens and cassegrain designs can both achieve high concentration ratios but the reflective cassegrain is not limited by chromatic aberration (<1000X limit) Shanks et al., 2015, 2016a; Languy et al., 2013. The cassegrain however typically has a lower acceptance angle due to the 2 reflective stages in comparison to the 1 refraction stage of the Fresnel lens (Shanks et al., 2015, 2016a). There has been much research into the cassegrain type concentrator (Dreger et al., 2014; Yehezkel et al., 1993; Chong et al., 2013; Chen and Ho, 2013; Victoria et al., 2013; McDonald et al., 2007; Roman et al., 1995; Terry et al., 1996, 2012) for its greater compactness (Roman et al., 1995; Miñano et al., 1995) and higher concentration ratios over the Fresnel Lens. Roman et al. (1995) and Yavrian et al. (2013) highlight the importance of optimising concentrator designs not only for optical efficiency but optical tolerance also.

Acceptance angles for high concentration systems are low (McDonald et al., 2007; Luque and Andreev, 2007; Akisawa et al., 2012; Chaves, 2008; Winston et al., 2005). However, research and careful design have been increasing the acceptance angle of high concentration photovoltaics (HCPV's) Dreger et al., 2014; Benitez et al., 2006. Benitez et al. (2006) designed a cassegrain reflector capable of 800× concentration ratio and an acceptance angle of ±0.86° but this and more systems still need to be experimentally tested. SolFocus has commercialised systems with an acceptance angle of ±1.4° (Winston et al., 2005) (McDonald et al., 2007; Chaves, 2008). OpSun have also performed outdoor measurements of three high concentration photovoltaics of geometrical concentration ratios 380X, 900X and 2250X, which gave acceptance angle valued of ±3.2°, ±1.9° and ±1.2° respectively (Yavrian et al., 2013). These commercial systems are however expensive and require highly accurate optics. In this paper ray trace simulations are carried out to optimise a cassegrain CPV design with respects to optical efficiency and acceptance angle. The simulation method also addresses realistic errors (such as surface roughness) which can occur in manufacturing. These uncertainties are not normally simulated despite the variety of modelling theory's and accuracy with which they can predict light behaviour (Schröder et al., 2011). As CPV research focuses towards achieving higher concentration ratios, the effect of these uncertainties will become increasingly important.

Untrue optimised designs can also occur depending on the simulation method and order of parameter determination. In a cassegrain concentrator many of the dimensions are linked and require to and fro optimisation of multiple variables together. This can become very complex if aiming for a specific geometric concentration, optical efficiency, irradiance distribution and overall size limit. In most cases there are a number of simplifying yet unrealistic assumptions made when performing ray trace simulations which can lead to significant losses within the built version of the system. The material, manufacturing method and location of the CPV device can significantly alter how it performs in comparison to the predicted simulations (Brogren et al., 2004; Fang et al., 2006; Guo et al., 2009; Han et al., 2008; Fernández et al., 2012).

2. Design method

The following study details the ray trace optimisation of a 500× cassegrain concentrator which was then built and tested to compare theoretical and experimental results. Parameters are optimised is stages with consideration to realistic conditions. This means the radius and width of the primary and secondary reflector dishes are determined first due to the 500× geometrical concentration requirement and shadowing effects of the secondary reflector. The focal lengths and separation distance of the two reflectors are then optimised but first with a reflective type homogenizer and then with a transparent homogenizer. The dimensions of the homogenizer are then refined further.

The optimisation criteria during simulations is to obtain a high optical efficiency and a well distributed irradiance upon the receiver over a range of at least ±1° tracking error. The effect of different attributes in the cassegrain design on the acceptance angle are characterised and an equation given for the minimum separation distance required to ensure all light from the primary reflector is intercepted by the secondary reflector. Typically, large focal lengths are required for good acceptance angles to be realised, however in this design we have obtained an acceptance angle of 1.2° for a primary reflector with focal length 200 mm. This in depth optimisation also allows for an optical efficiency of >55% to be maintained up to ±1.5° tracking error.

More importantly, the simulation method presented in this paper considers the surface quality of the optical components, the surface structure of the reflective and refractive optics are modelled using their material bidirectional scattering distribution function (BSDF). The BSDF is associated with the surface roughness through the total integrated scatter (TIS) of optical interfaces and dictates how light is transmitted or reflected from it. The BSDF is the combined function of the bidirectional reflectance distribution function (BRDF) and the bidirectional transmittance distribution function (BTDF). The BSDF is generally in the form of a mathematical formula, often encompassing discrete samples of measured data, which approximately models the actual surface behaviour. The bidirectional scattering distribution function radiometrically characterizes the scatter of light from a surface as a function of

the angular positions of the incident and scattered rays (Asmail, 1991; Breault Research Organization, 2012). A range of BSDF's are used in these simulations for the reflective and refractive components to represent the possible optical finishes they may have depending on material and manufacturing process. The BSDF's used are company provided models which are available in the ray tracing software ASAP's library of materials and associated light scattering profiles.

During the experimental testing, the dielectric material of the homogenising optic was found to be the source of significant loss due to poor stability and surface finish. The acceptance angle of the design was however proved and measurements excluding the homogeniser loss validated the performance of the primary and secondary reflectors. Of which, the primary reflector was manufactured out of plastic for an improved surface finish, weight and reduced cost. The experimental testing confirmed the materials use as a primary optical component in CPV technology.

3. Design Concept and geometric concentration ratio

A two-stage reflector type concentrator was explored due to the advantages of compactness and having an upward facing receiver (Welford and Winston, 1989). With the receiver situated in the base of the primary reflector (See Fig. 1), passive cooling methods are easier employed and the cell temperature is more manageable. The basic design for this solar concentrator employs a cassegrain set up of two parabolas (McDonald et al., 2007) as shown in Fig. 1. For this study we will be aiming for a geometric concentration ratio of 500× which requires, for a solar cell of 1 cm^2, an input area of at least 500 cm^2. This must also take into account the shadowing effect of the secondary reflector.

In ideal conditions this set up should produce a concentrated uniform irradiance distribution upon a solar cell placed in the base of the 1st reflector. Light rays from the sun however are not parallel and have a small divergence of ±0.27°, resulting in a diffused focusing point. This can be compensated for by adjusting the reflective dishes to be afocal, so they are no longer coincident, and finding the optimum position of the secondary reflector with respects to the primary reflector and receiver.

The focal point, f, radius, r, and depth, y, of a parabola are related through Eq. (1) (McDonald et al., 2007).

$$r^2 = 4fy \tag{1}$$

where the focal length can be related to the Radius of Curvature (ROC), through Eq. (2), which should be noted is not the same as the curvature, k, which can be defined as the rate of change of the angle θ with respect to the distance, s, travelled along the curve (Victoria et al., 2013).

$$2f = ROC = \frac{1}{k} = \frac{1}{|\partial\theta/\partial s|} \tag{2}$$

From Eq. (2) it can be assumed a lower curvature produces a better tolerance to error. Wither the error is in incident light angle or curve manufacturing. A larger focal length is hence desired for a better acceptance angle, however the secondary reflector focal length and curvature will also have an effect.

From Fig. 1, the reflector dimensions can be related through angle A, the maximum value of θ which light rays can make with the vertical and still pass through the focal point. It determines the utmost limit that light can strike the inside curve of the primary reflector and is related to the reflector's parabolic parameters via Eq. (3) (Roman et al., 1995).

$$\frac{f_1}{2r_1} = \frac{1}{4\tan(A/2)} = \frac{f_2}{2r_2} \tag{3}$$

Angle A links both reflectors dimensions to each other when they are coincident. When they are not coincident Eq. (3) no longer holds and care must be taken to ensure the secondary reflector still accommodates all rays being reflected with angle A. It should also be noted that square cut parabolic reflectors were chosen for the primary collector and secondary reflector in order to increase the packing factor when the primary reflectors are arranged side by side in an array system. The width, w, of a reflector is related to

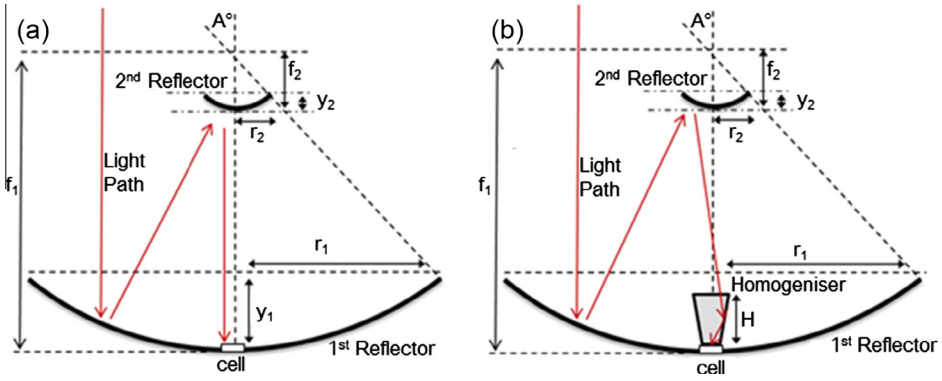

Fig. 1. Diagrams of the theoretical path for parallel light incident on a parabolic reflector, reflecting towards the focal point and then reflecting from the 2nd parabolic reflector to (a) become parallel again or (b) focus on the surface of a homogeniser.

the radius, r, through Pythagoras as shown in Fig. 2 and is now the one of the main factors determining how much light with angle A is captured.

To efficiently capture the light from reflected from the primary dish, the secondary dish should be as large as possible with a large focal length to improve acceptance angle, according to Eq. (2). However, to large a secondary component will cause significant shadowing, increasing the primary reflectors width to maintain 500× geometric concentration and increase strain on the cover glass to which the secondary is attached. The width of the secondary reflector was hence chosen to be a maximum of 50 mm as a suitable size and weight that will not incur excessive shadowing or difficulties in manufacturing and assembly. The following relationship was then formed to calculate the separation distance (SD) between the two reflectors required to collect all rays given the secondary reflector width and primary collector focal length and radius:

$$SD = f_1 - \left(\frac{0.5w}{\tan\left(2\tan^{-1}\left(\frac{r_1}{2f_1}\right)\right)} \right) \quad (4)$$

The radius of the primary reflector, r_1, is also dependent on the width, w, to ensure a geometric concentration ratio of 500× is reachable. In this way, taking w as 50 mm, results in a r_2 of 35.4 mm and r_1 of 162.6 mm as illustrated in Fig. 2.

4. Effect of separation distance on optical tolerance

Combinations of varying primary and secondary reflector focal lengths were carried out next, investigating the displacement of the final ray positions due to a 1° tracking error. The secondary reflector width, w was taken as 50 mm, r_1 as 162.6 mm, f_1 was varied between 150 and 220 mm and f_2 varied between 50 and 80 mm The separation distance was also changed as discussed earlier, calculated using Eq. (4) above, to accommodate all rays from the primary reflector.

Larger separation distances result in lower ray displacement and hence a higher tracking tolerance as shown in Fig. 3. There is a cluster of results situated at a ray displacement of ~10 mm, this is due to the light rays focusing before the receiver and diverging out in all directions including towards the receiver and the normal. The separation distance is linked to the primary reflector focal length which counter intuitively (Eq. (2)) must be decreased to gain a better optical tolerance by increasing the separation distance (Eq. (4) and Fig. 3). Next, the homogeniser is introduced to allow for a larger separation distance and improve the irradiance uniformity upon the cell. The homogeniser is of a square pyramid shape, positioned upside down without a point as shown in Fig. 1 and later in Fig. 5. It can be made of either metal with reflective inside walls or can be a solid transparent homogeniser so

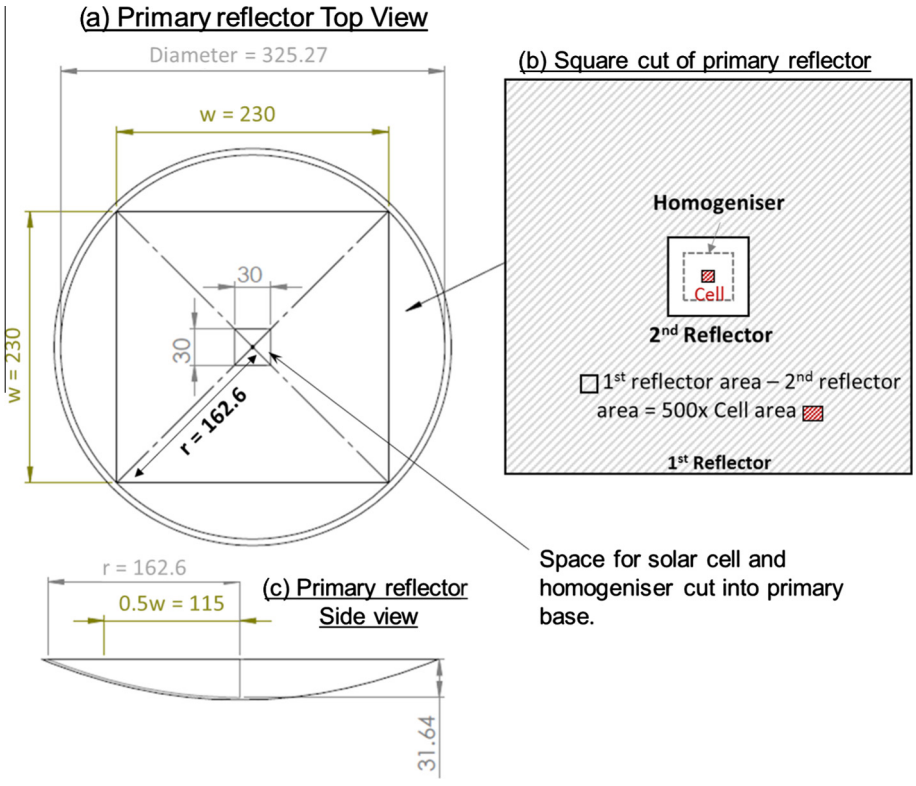

Fig. 2. Schematic of square cutting and shape matching of reflectors, homogeniser and solar cell. All dimensions are given in mm. (a) Top view of inside square cut of original circular primary reflector dish with a square hole in the base for the receiver assembly and homogeniser. (b) Top view of all square components in central alignment with the solar cell. (c) Side view of original circular primary reflector from (a) showing depth, radius and resulting half width after square cut.

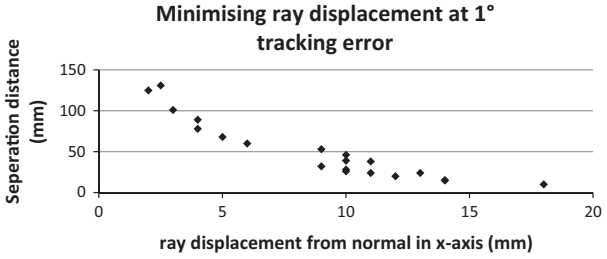

Fig. 3. Graph of separation distance against ray displacement from position of normal alignment with the sun due to a tracking error of 1°. Displacement measurements only taken in *x*-axis but due to the symmetry of the system represent the displacement incurred in *y*-axis as well.

as to take advantage of total internal reflection (TIR) at the sloped sides of the homogeniser.

5. Effect of homogeniser

Taking the same range of focal lengths as used before for the separation distance investigation but focusing simulations to the ~200 mm and ~70 mm focal length combination, rough dimensions of the homogeniser were next determined. The focal lengths of the primary concentrator and secondary reflector were investigated with a metal homogeniser (mirrored sides), aiming for high optical efficiencies. The reflectivity of the homogeniser walls were initially taken to be 95% for the optimisation procedure and a shortlist of parameter combinations were found from various simulation testing and shown in Fig. 4(a) below.

The initial optical efficiency at normal incidence in Fig. 4 (a) is due to the reflection loss at the primary reflector, secondary reflector, and third stage homogeniser. The sharp decline in optical efficiency from 1° to 1.5° seen is due to an increase in the number of reflections within the homogeniser, each costing 5% of optical efficiency (reflective losses), and because of light passing by the homogeniser (diverging by >10 mm). The acceptance angle can hence be increased by using a transparent solid homogeniser, which utilises total internal reflection to direct the rays towards the receiver and optimising the width. For this, the parameters obtaining the highest optical efficiency at normal incidence (f1 = 200 mm, f2 = 70 mm and H = 70 mm from Fig. 4(a)) were investigated further for optimisation as shown in Figs. 4(b) and 6. The optimum parameters from Fig. 4(b) were found to be that of f1 = 200 mm, f2 = 70 mm, H = 75 mm and SD = 162 mm.

Ideally the output face of the homogeniser, where the receiver is placed, is the exact size of the receiver to avoid loss. An output face of 10.1 mm × 10.1 mm was taken, instead of 10 mm × 10 mm as a tolerance measure and the homogenisers height and entry aperture width were optimised further (Figs. 5 and 6).

For maximum acceptance angle, the light rays reflected from the secondary reflector should come to a focus upon entering the homogenisers input surface and the input surface width should be large enough to collect offset rays due to tracking errors (Fig. 5). Increasing the width however also decreases the gradient of the sloped sides, resulting in more rays not meeting the criteria for TIR and passing through the walls of the homogeniser (Fig. 5b). This can be balanced by expanding the height of the homogeniser, but again this tends to an increasing number of rays being lost due to more incurred reflections. Various parameter combinations were investigated in an attempt to find the optimum scenario (Fig. 6).

The most promising system parameter combination for tracking tolerance was chosen to be that with a homogeniser height of 75 mm, an input width of 30 mm and a separation distance between the two reflectors of 162 mm. This configuration maintains an optical efficiency of 84.82–81.89% over ±1° tracking error and 55.49% optical efficiency at a tracking error of 1.5°. This is assuming a reflection loss of 5% at the primary and secondary and hence could be higher or lower depending on the mirror quality. The surface quality of the reflective dishes and the refractive homogeniser will both have an effect on the final optical efficiency of the system and is discussed further in the practical considerations and error analysis section.

The irradiance distribution of each set of parameter configurations was also recorded, all of which followed a

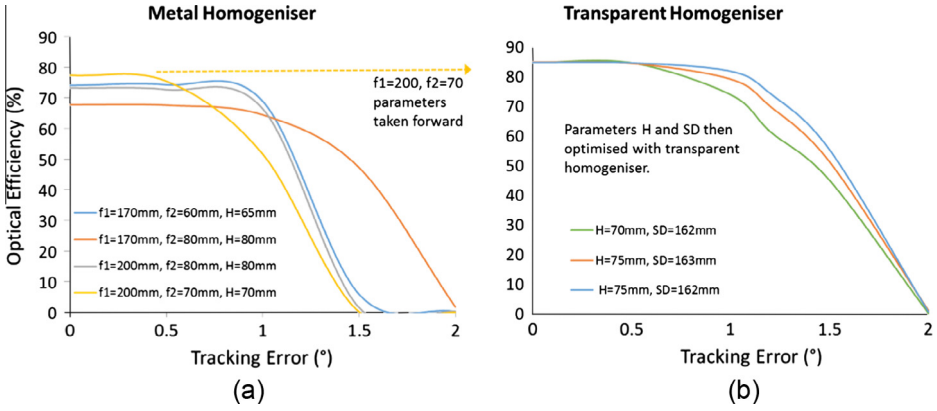

Fig. 4. Graph of optical efficiency as tracking error is increased in the horizontal axes whilst using (a) a metal homogeniser and (b) a solid transparent homogeniser. Where f1 and f2 are the focal lengths of the primary and secondary reflectors, H represents the height of the homogeniser and SD represents the Separation Distance between the two reflectors. In (b) f1 and f2 are 200 mm and 70 mm for all 4 results with varying H and SD.

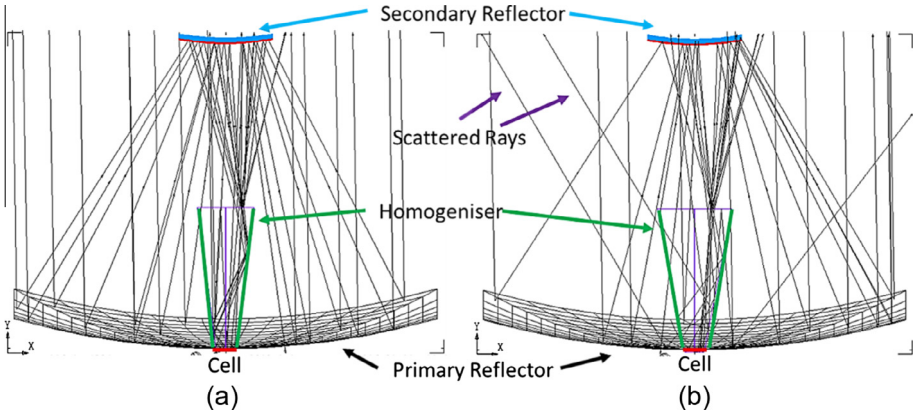

Fig. 5. 3D ray trace diagrams of rays with an incidence angle of 1° and a solid transparent homogeniser with (a) the optimised homogeniser dimensions and (b) showing an increased homogeniser input width (which results in more rays refracting out of the homogeniser instead of undergoing TIR).

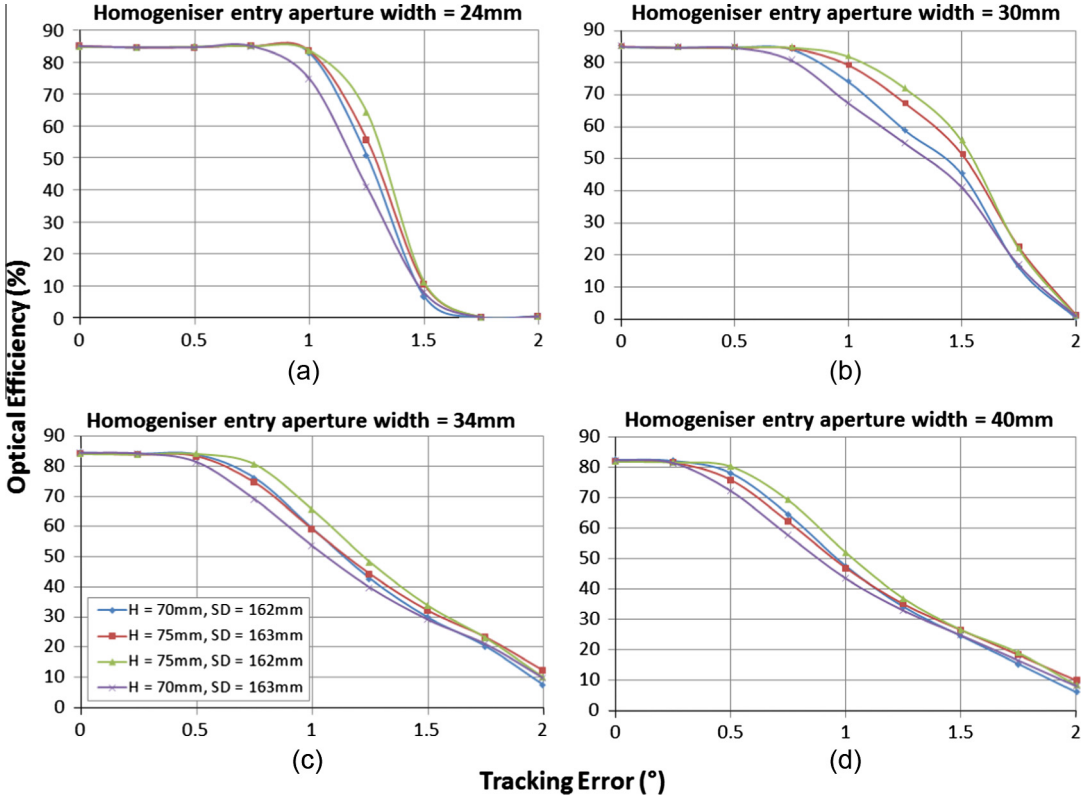

Fig. 6. Graph of resulting tracking tolerance from different combinations of homogeniser parameters and separation distance where H represents Homogeniser height in mm, W represents the input face width in mm and the separation distance, SD, is either 163 mm or 162 mm.

similar trend with increasing tracking error as shown below in Fig. 7.

The crossed pattern observed in Fig. 7(a), is due to less light reflecting directly from the corners of the homogeniser walls. The flux distribution at normal incidence is relatively well distributed and although this declines with increasing tracking error as expected, the change in irradiance across the cell is gradual, there are no sharp peaks of high irradiance. From Fig. 7 above it can be seen the maximum flux increases with tracking error, from 0.585 W/sq-mm in (a) to 0.723 W/sq-mm in (b) and 1.1 W/sq-mm in Fig. 7(c), before returning down to 0.441 W/sq-mm in (c). The *x*-axis and *z*-axis flux profiles however remain at a gradual incline. As the tacking error increases the light rays are reflected first by one of the side walls of the homogeniser then by both, shifting the irradiance distribution from one corner of the cell through to the other side, depending on the direction the tracking error is incurred. At 1.5° tracking error, Fig. 7(d), roughly half of the light rays are lost by not being captured by the homogeniser at the entry aperture, or reflecting at an angle greater than that for TIR.

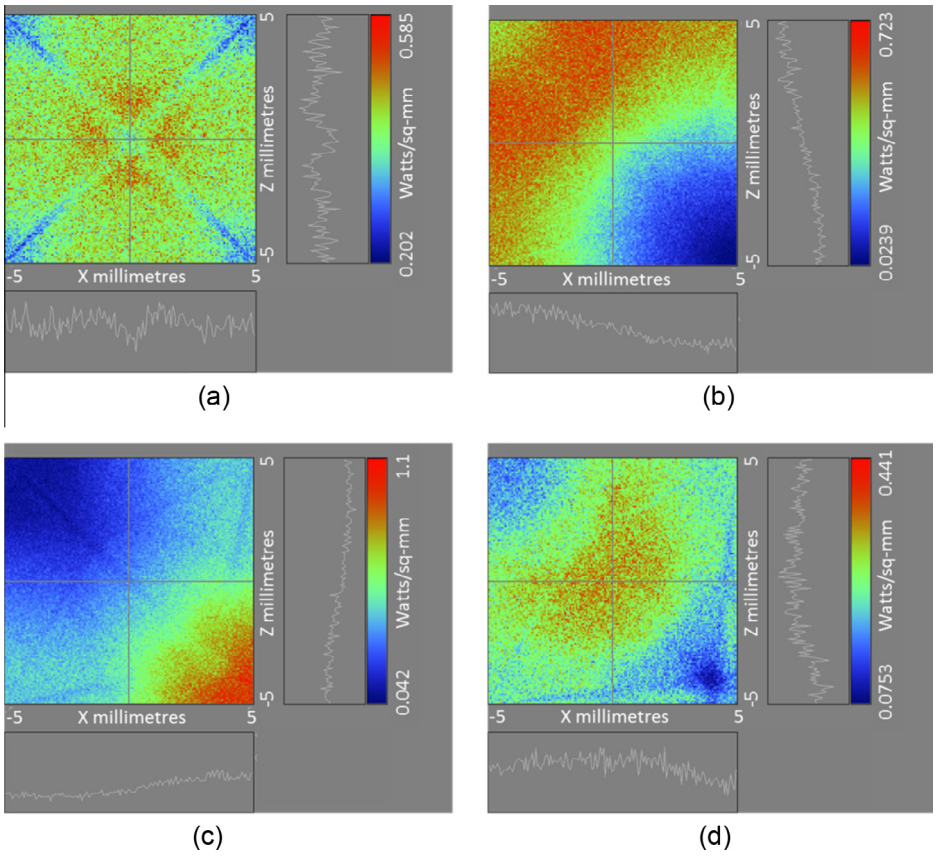

Fig. 7. The irradiance distribution upon the receiver with increasing tracking error for the chosen system parameter configuration with: (a) No tracking error; (b) 0.5° tracking error; (c) 1° tracking error and (d) 1.5° tracking error.

6. Practical considerations and error analysis

6.1. Dimensional and alignment errors due to manufacturing

Possible errors in the dimensions of the individual components have been considered in the design process of the proposed system. Errors in the width of the primary collector and secondary reflector will affect the geometrical concentration ratio and possibly the tracking tolerance range if large enough. Errors in the horizontal alignment of the two parabolic reflectors will have a similar effect to tracking error so are not as detrimental due to the use of the homogeniser but would offset the optical efficiency shown in Fig. 6 by the horizontal error incurred. The vertical error in the separation distance between the primary collector and secondary reflector can decrease the optical efficiency but the effect is only noticeable at tracking errors >0.5° and is still relatively small at ±1° error as shown in Fig. 6. The optical efficiency can drop from 81.89% to 79.21% due to a ±1 mm vertical error at a tracking error of ±1°. The accuracy of the homogenisers' exit aperture dimensions (Fig. 8) and its alignment with the cell are the main sources of loss when considering dimensional and alignment errors for this design.

Perfect alignment with the cell and a homogeniser exit aperture of 10 × 10 mm obtains a maximum of 86.46% optical efficiency. With a 0.1 mm alignment tolerance, the exit aperture dimensions, 10.1 mm × 10.1 mm, produces a maximum of 84.82% optical efficiency and decreases by ~1.7% (absolute value) for every 0.1 mm increase in the area dimensions as shown in Fig. 8. At present time, moulds of the homogeniser are achieving an accuracy of ±0.2 mm, resulting in an uncertainty of ±3.3% optical efficiency (absolute value).

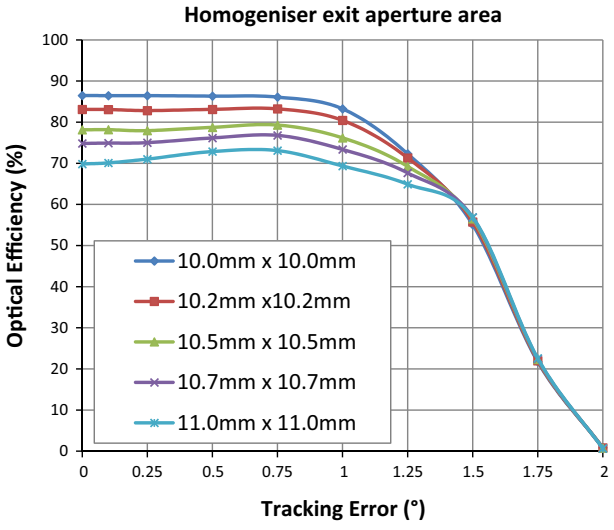

Fig. 8. Varying homogeniser output face area and the effect on optical efficiency with increasing tracking error.

6.2. Material and surface imperfections

Fig. 9 confirms that no light rays are lost within the system at normal incidence as shown by the 'ideal' scenario results. Although a reflectance loss of 5% was assumed for finding the optimum design requirements, manufacturing limitations in the prototyping stage may result in a lower reflectance. When simulating the primary and secondary reflectors with a BSDF of polished aluminium there is around 10% reflectance loss at both surfaces. The focus of the rays also widens due to the increase in scattering from these two surfaces. This reflection loss on both dishes causes a significant drop in optical efficiency as shown in Fig. 9. There are materials and coatings with improved reflectance (Shanks et al., 2015) such as silver (~97% reflectance) but degradation and/or expense are common problems with such high quality optics. On entering the homogeniser, there is a small amount of energy loss where some light is reflected away instead of refracting into the dielectric material. This can be improved with antireflection coatings and special textures of the homogeniser surface but again this is expensive (Huang et al., 2012; Zhou et al., 2013). The surface roughness of the homogeniser is a main factor causing a drop in optical efficiency and lowering the acceptance angle depending on the material used in manufacturing. There is a severe drop especially for the BSDF's related to poorer surface finishes as shown in Fig. 9. These BSDF's were selected from a database of expected BSDF's of optical finishes available from companies. The BSDF's were chosen simply to give a good range. Typical surface quality would be expected to be in the upper region of these samples. More accurate solar trackers and accurately built systems would not suffer as significantly if within ±0.5° accuracy but these incur further expense as well.

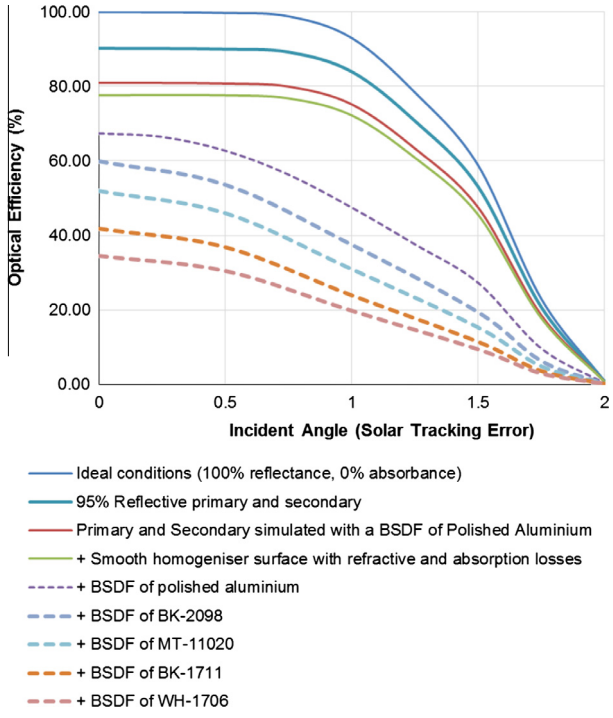

Fig. 9. Practical losses summary. Optical efficiency decreases as realistic surface losses are added in stages. The dashed lines represent possible surface finishes of the homogeniser depending on which material and manufacturing process is employed (Shanks et al., 2016b).

7. Manufacturing of prototype

In this study, a primary reflector dish was computer numerical control (CNC) machined out of a high temperature form of ABS plastic to take advantage of the lightweight and surface smoothness of the material. The dish was then vacuum metallised and a reflectance of ~90% measured. The secondary reflector was made of solid aluminium due to the high concentration of light and temperature it would be subject to. Similarly this was CNC'd but then polished. The homogeniser was moulded using sylgaurd which had a measured absorbance of ~6% over the working wavelength range of the solar cell to be used but the overall optical efficiency depends on the surface structure and angle of incident light when entering the homogenizer (some reflection loss and scattering). A prototype of the optimum design was manufactured as a 3 by 3 module as shown in Fig. 10 below.

8. Experimental investigation

The module was tested by the Helios 3198 solar simulator (Fig. 11) Domínguez et al., 2008 at the Centre for

Fig. 10. Photo of 3 by 3 cassegrain concentrator prototype from (a) top view and (b) side view. (a) Shows the concentration of sunlight onto the homogenisers and solar cells.

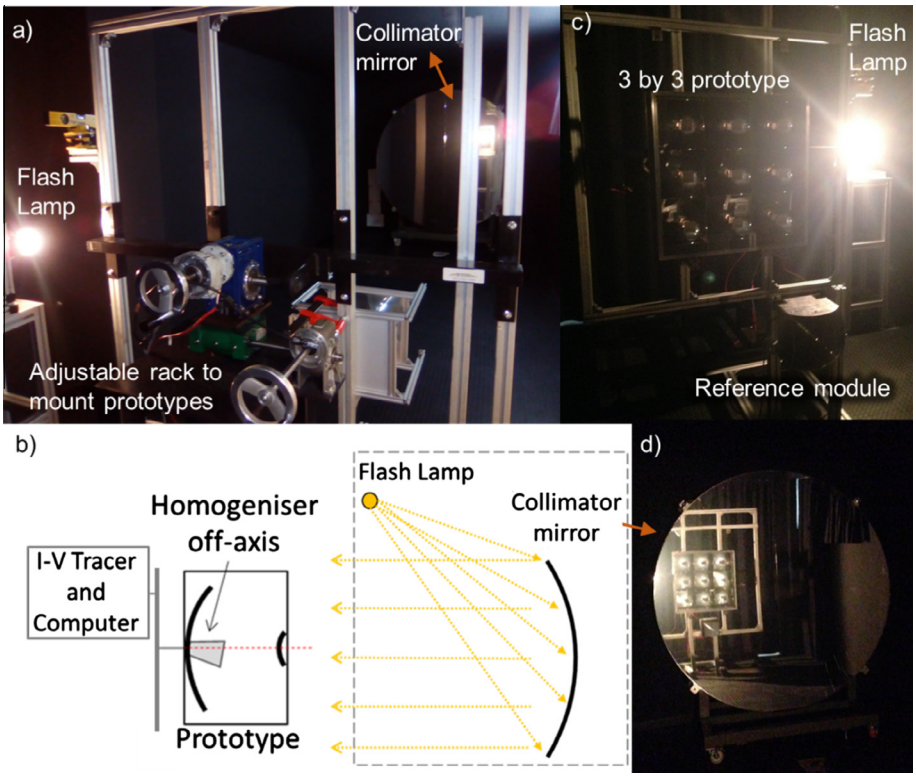

Fig. 11. (a) Photo of Helios 3198 solar simulator taken from behind adjustable mounting rack showing flash lamp and collimator mirror. (b) Schematic diagram showing set up of solar simulator and the tilting homogeniser within the prototype when mounted. (c) Photo of 3 by 3 prototype mounted on rack for testing. (d) Photo of collimator mirror on opposite of the room with reflection of prototype.

Advanced Studies in Energy and Environment (CEAEMA) at the University of Jaen in Southern Spain (Fernández et al., 2012) under 850 W/m^2. The Helios has a collimation angle of ±0.4° and matches the spectrum of AM1.5D. It is a very powerful flash simulator for measuring the performance of concentrator photovoltaic modules and allows accurate analysis of the acceptance angle of such modules (Domínguez et al., 2008).

Initial measurements showed challenges with the stability of the Homogeniser optic. Due to the small contact area of the homogeniser with the solar cell and base (10 × 10 mm contact area), and the flexibility of the material used (sylgaurd), when the full system was rotated towards the solar simulator (Fig. 11) the homogeniser also leaned out of alignment with the primary and secondary reflectors (shown in Fig. 11). Further investigation with the homogeniser optic proved it has an increased optical loss resulting in the full system only performing at ~40% optical efficiency instead of the anticipated ~65% at normal incidence (Fig. 12). The output of the measured system as the misalignment angle was increased did not drop as sharply as expected from the results suggested in Fig. 9. This suggests that the homogeniser has a surface scattering profile close to that of BK-1711 in Fig. 9 but the tilting issue and perhaps the connecting medium to the solar cell reduces the normal incidence maximum. The experimental measurements shown in Fig. 12 however confirm the acceptance angle of the designed system.

Equivalent measurements were taken without the homogeniser and instead a solar cell of increased size used at the position of the homogenisers entry aperture (where the light focuses). This test proves the efficiency of the primary and secondary reflectors follows simulation predictions and only the homogenising optic needs replacement. The acceptance angle without the homogeniser however is much smaller as expected and the maximum optical efficiency at normal incidence is slightly increased due to the removal of the homogenisers refractive losses (Fresnel reflection upon entry, absorption, scattering). A higher optical grade glass homogeniser would increase the acceptance angle of these practical results which would then lead to an expected performance similar to the uppermost curve in Fig. 12. This will be the next step of experimental testing as well as increasing the geometric concentration ratio to 1500× with use of a smaller solar cell and redesigned homogenising optic.

9. Conclusion

The tracking tolerance and optical efficiency of a cassegrain type solar concentrator was optimised through the use of ray trace analysis to achieve high optical efficiencies of 84.82% at normal incidence, 81.89% at ±1° tacking error and 55.49% at ±1.5° tracking error for high optical grade components. The optimised design was found to be with a primary parabolic reflector of focal length 200 mm and

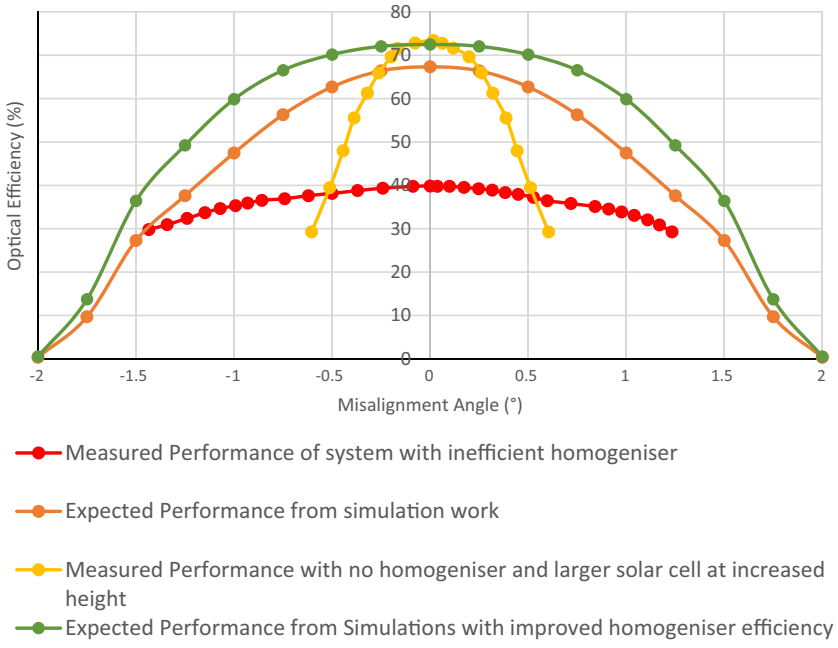

Fig. 12. Comparison of Expected performance from simulation and real case measured performance.

a secondary inverse parabolic reflector of focal length 70 mm placed 162 mm from the primary collector. The optimised system required a solid transparent homogeniser of height 75 mm with an entry aperture of 30 mm × 30 mm and exit aperture of 10 mm by 10 mm. The use of the homogeniser not only improves the tracking tolerance and the irradiance distribution but also allows more flexibility in the manufacturing and assembly of the design. The detailed characterisation of the proposed system, as well as the separation distance equation, may be beneficial in the design of parabolic reflector systems. It may also benefit single stage lens systems (that focus onto a homogeniser), as a guideline to help improve an aspect of the system dependent on alignment, focusing area or uncertainties. Manufacturing uncertainties were considered and the material and surface structure of the homogeniser in particular proved to be the biggest source of loss. This was confirmed in experimental tests of the prototype where the module produced 40% of the ideal 500× power output from the cell instead of the anticipated ~65% from simulation work. However, the designed acceptance angle of ~1° appears to be confirmed. The primary and secondary reflectors follow simulation predictions in performance and redirect the light to the desired focusing area with ~90% reflectance efficiency. This is a key result as reflective optics of a specific 3D shape are not always manufactured accurately at the prototype stage for an acceptable cost. This result also validates the ABS plastic material for use as a CPV primary optic and reinforces the benefit of investigating more materials for CPV applications. Further outdoor testing is required over prolonged periods and a remodel of the homogeniser with a 5.5 × 5.5 mm solar cell will be carried out to increase the geometric concentration ratio to 1500×.

Acknowledgments

This work has been carried out as a part of BioCPV project jointly funded by DST, India (Ref No: DST/SEED/INDO-UK/002/2011) and EPSRC, UK, (Ref No: EP/J000345/1). J.P. Ferrer-Rodriguez is supported by the Spanish Economy Ministry and the European Regional Development Fund/Fondo Europeo de Desarrollo Regional (ERDF/FEDER) under the project ENE2013-45242-R. Authors acknowledge the funding agencies for the support. In support of open access research all underlying article materials (such as data, samples or models) can be accessed upon request via email to the corresponding author.

References

Akisawa, A., Hiramatsu, M., Ozaki, K., 2012. Design of dome-shaped non-imaging Fresnel lenses taking chromatic aberration into account. Sol. Energy 86, 877–885. http://dx.doi.org/10.1016/j.solener.2011.12.017.

Asmail, C., 1991. Bidirectional scattering distribution function (BSDF): a systematized bibliography. J. Res. Natl. Inst. Stand. Technol. 96, 215. http://dx.doi.org/10.6028/jres.096.010.

Benitez, P., Cvetkovic, A., Winston, R., Reed, L., 2006. New High-Concentration Mirror-Based Kohler Integrating Optical Design for Multijunction Solar Cells. Int. Opt. Des., Washington, D.C.: OSA; p. TuD3. http://dx.doi.org/10.1364/IODC.2006.TuD3.

Breault Research Organization. ASAP Technical Guide: Scattering in ASAP 2012:17–21. http://www.breault.com/sites/default/files/knowledge_base/brotg0922_scatter_1.pdf (accessed October 12, 2015).

Brogren, M., Helgesson, A., Karlsson, B., Nilsson, J., Roos, A., 2004. Optical properties, durability, and system aspects of a new aluminium-polymer-laminated steel reflector for solar concentrators. Sol. Energy Mater. Sol. Cells 82, 387–412. http://dx.doi.org/10.1016/j.solmat.2004.01.029.

Chaves, J., 2008. Introduction to Nonimaging Optics. CRC Press.

Chen, Y.T., Ho, T.H., 2013. Design method of non-imaging secondary (NIS) for CPV usage. Sol. Energy 93, 32–42. http://dx.doi.org/10.1016/j.solener.2013.03.013.

Chong, K.K., Lau, S.L., Yew, T.K., Tan, P.C.L., 2013. Design and development in optics of concentrator photovoltaic system. Renew. Sustain. Energy Rev. 19, 598–612. http://dx.doi.org/10.1016/j.rser.2012.11.005.

Domínguez, C., Antón, I., Sala, G., 2008. Solar simulator for concentrator photovoltaic systems. Opt. Express 16, 14894–14901. http://dx.doi.org/10.1364/OE.16.014894.

Dreger, M., Wiesenfarth, M., Kisser, A., Schmid, T., Bett, A.W., 2014. Development and investigation of a CPV module with cassegrain mirror optics. CPV-10.

Fang, H., Guo, P., Yu, J., 2006. Surface roughness and material removal in fluid jet polishing. Appl. Opt. 45, 4012–4019. http://dx.doi.org/10.1364/AO.45.004012.

Fernández, E.F., Pérez-Higueras, P., Garcia Loureiro, A.J., Vidal, P.G., 2012. Outdoor evaluation of concentrator photovoltaic systems modules from different manufacturers: first results and steps. Prog. Photovoltaics Res. Appl. http://dx.doi.org/10.1002/pip.1262, n/a – n/a.

Goldstein, A., Gordon, J.M., 2011. Tailored solar optics for maximal optical tolerance and concentration. Sol. Energy Mater. Sol. Cells 95, 624–629. http://dx.doi.org/10.1016/j.solmat.2010.09.029.

Gordon, J.M., Katz, E.a., Feuermann, D., Huleihil, M., 2004. Toward ultrahigh-flux photovoltaic concentration. Appl. Phys. Lett. 84, 3642. http://dx.doi.org/10.1063/1.172369.

Gordon, J.M., Feuermann, D., Young, P., 2008. Unfolded aplanats for high-concentration photovoltaics. Opt. Lett. 33, 1114–1116.

Guo, S., Zhang, G., Li, L., Wang, W., Zhao, X., 2009. Effect of materials and modelling on the design of the space-based lightweight mirror. Mater. Des. 30, 9–14. http://dx.doi.org/10.1016/j.matdes.2008.04.056.

Han, J.-Y., Kim, S.-W., Han, I., Kim, G.-H., 2008. Evolutionary grinding model for nanometric control of surface roughness for aspheric optical surfaces. Opt. Express 16, 3786–3797. http://dx.doi.org/10.1364/OE.16.003786.

Huang, C.K., Sun, K.W., Chang, W.-L., 2012. Efficiency enhancement of silicon solar cells using a nano-scale honeycomb broadband antireflection structure. Opt. Express 20, A85–A93.

Languy, F., Habraken, S., 2013. Nonimaging achromatic shaped Fresnel lenses for ultrahigh solar concentration. Opt. Lett. 38, 1730–1732.

Languy, F., Lenaerts, C., Loicq, J., Thibert, T., Habraken, S., 2013. Performance of solar concentrator made of an achromatic Fresnel doublet measured with a continuous solar simulator and comparison with a singlet. Sol. Energy Mater. Sol. Cells 109, 70–76. http://dx.doi.org/10.1016/j.solmat.2012.10.008.

Luque, A., Andreev, V.M., 2007. Concentrator photovoltaics. http://dx.doi.org/10.1007/978-3-540-68798-6.

McDonald, M., Horne, S., Conley, G., 2007. Concentrator design to minimize LCOE; 6649:66490B – 66490B – 11. http://dx.doi.org/10.1117/12.735738.

Miñano, J.C., Gonźlez, J.C., Benítez, P., 1995. A high-gain, compact, nonimaging concentrator: RXI. Appl. Opt. 34, 7850–7856. http://dx.doi.org/10.1364/AO.34.007850.

Roman, R.J., Peterson, J.E., Goswami, D.Y., 1995. An off-axis cassegrain optimal design for short focal length parabolic solar concentrators. J. Sol. Energy Eng. 117, 51. http://dx.doi.org/10.1115/1.2847742.

Schröder, S., Duparré, A., Coriand, L., Tünnermann, A., Penalver, D.H., Harvey, J.E., 2011. Modeling of light scattering in different regimes of surface roughness. Opt. Express 19, 9820–9835. http://dx.doi.org/10.1364/OE.19.009820.

Shanks, K., Senthilarasu, S., Mallick, T.K., 2015. High-Concentration Optics for Photovoltaic Applications. In: Pérez-Higueras, P., Fernández, E.F. (Eds.), High Conc. Photovoltaics Fundam. Eng. Power Plants, 1st ed. Springer International Publishing, Cham, pp. 85–113. http://dx.doi.org/10.1007/978-3-319-15039-0.

Shanks, K., Senthilarasu, S., Mallick, T.K., 2016a. Optics for Concentrating Photovoltaics: trends, limits and opportunities for materials and design. Renew. Sustain. Energy Rev. 60, 394–407.

Shanks, K., Baig, H., Senthilarasu, S., Reddy, K.S., Mallick, T.K., Baig, H., et al., 2016b. Conjugate refractive–reflective homogeniser in a 500× cassegrain concentrator: design and limits. IET Renew. Power Gener., 1–8 http://dx.doi.org/10.1049/iet-rpg.2015.0371.

Terry, C.K., Peterson, J.E., Goswami, D.Y., 1996. Feasibility of an iodine gas laser pumped by concentrated terrestrial solar radiation. J. Sol. Energy Eng. 118, 136. http://dx.doi.org/10.1115/1.2848006.

Terry, C.K., Peterson, J.E., Goswami, D.Y., 2012. Terrestrial solar-pumped iodine gas laser with minimum threshold concentration requirements. J. Thermophys. Heat Transf.

Victoria, M., Dominguez, C., Askins, S., Anton, I., Sala, G., 2013. Experimental analysis of a photovoltaic concentrator based on a single reflective stage immersed in an optical fluid. Prog. Photovoltaics Res. Appl. http://dx.doi.org/10.1002/pip.2381.

Welford, W.T., Winston, R., 1989. High Collection Nonimaging Optics. Elsevier. http://dx.doi.org/10.1016/B978-0-12-742885-7.50002-4.

Winston, R., Miñano, J.C., Benítez, P., Shatz, N., Bortz, J.C., 2005. Nonimaging Optics. Elsevier. http://dx.doi.org/10.1016/B978-012759751-5/50013-0.

Yavrian, A., Tremblay, S., Levesque, M., Gilbert, R., 2013. How to increase the efficiency of a high concentrating PV (HCPV) by increasing the acceptance angle to ±3.2°. 9TH Int. Conf. Conc. Photovolt. Syst. CPV-9. AIP Conf. Proc., vol. 1556, p. 197–200. http://dx.doi.org/10.1063/1.4822230.

Yehezkel, N., Appelbaum, J., Yogev, a., Oron, M., 1993. Losses in a three-dimensional compound parabolic concentrator as a second stage of a solar concentrator. Sol. Energy 51, 45–51. http://dx.doi.org/10.1016/0038-092X(93)90041-L.

Zhou, G., He, J., Xu, L., 2013. Antifogging antireflective coatings on Fresnel lenses by integrating solid and mesoporous silica nanoparticles. Microporous Mesoporous Mater. 176, 41–47. http://dx.doi.org/10.1016/j.micromeso.2013.03.038.